Thermo-cross-linkable fullerene for long-term stability of photovoltaic devices

Journal Name

ARTICLE

Thermo-cross-linkable fullerene for long-term stability of photovoltaic devices

Received 00th January 20xx,
Accepted 00th January 20xx

DOI: 10.1039/x0xx00000x

www.rsc.org/

Nabankur Deb [a], Raghunath R. Dasari [b], Karttikay Moudgil [b], Jeff L. Hernandez [b], Seth R. Marder [a,b,c], Yan Sun [d], Alamgir Karim [d] and David G. Bucknall [a,c,e *]

In this study, a highly soluble PCBM-based thermo-cross-linkable fullerene precursor has been synthesized for use in in bulk heterojunction based organic solar cells. The cross-linking was achieved using a thermally activated benzocyclobutene (BCB) molecule. The thermo-crosslinking reaction is initiated at temperatures as low as 150 °C. Compared to PCBM, the cross-linked fullerene is highly insoluble and has a diffusional mobility in poly(3-hexylthiophene) (P3HT) which is an order of magnitude slower than PCBM. Its electron mobility is comparable to that of PCBM and organic photovoltaic (OPV) devices consisting of bulk heterojunction active layers with P3HT and this fullerene show very similar efficiencies. Devices prepared either with pure cross-linked fullerene or its mixture with PCBM as acceptors in OPVs have been shown to be highly stable to accelerated aging with little loss in device efficiency up to 48 hours of aging at 150 °C. This compares to a loss of 60% of initial efficiency in identically prepared devices when using PCBM as the acceptor. Optical microscopy and grazing incidence wide angle x-ray scattering (GIWAXS) shows that a probable cause for this excellent stability in the cross-linked fullerene containing BHJs is associated with a significant inhibition of formation of crystals of fullerene.

Introduction

The discovery of highly efficient charge transfer from semiconducting polymers to electron accepting C_{60} fullerenes in OPVs[1] has led to the widespread use of fullerenes in the field of organic electronics.[2-5] The limited solubility of unmodified C_{60} led to the synthesis of new methanofullerene derivatives such as [6,6]-phenyl-C_{60}-butyric methyl ester (PCBM)[2], which were more soluble, as well as more efficient electron acceptors in OPVs. PCBM has since become one of the most popular fullerene acceptors and has been used in a variety of high performing organic photovoltaics (OPVs).[3-5] In the active layer i.e. the bulk hereterojunction (BHJ) layer, the conjugated polymer-fullerene mixture attains a complex phase behavior as a result of the solution processing and subsequent thermal annealing. In blends, poly(3-hexylthiophene) (P3HT) and PCBM fullerene phase segregate and tend to initially form[6] nano-scale aggregates which increase in size during post-processing thermal annealing and are associated wth improving device mobility and performance.[7] However, annealing at such temperatures for longer periods of time or accelerated aging, leads to formation of micro-scale (micrometer-sized) fullerene aggregates, which have been shown to be the underlying pathway for eventual device degradation.[8-10] To counter these effects and in particular to prevent or reduce fullerene aggregation, a number of approaches have been implemented including use of fullerene mixtures,[10, 11] modified fullerenes for supramolecular interactions,[12] in-situ polymerization of the fullerene,[13] UV assisted oligomerization of the fullerene in the BHJ,[14, 15] solution blending of soluble chemically-derived dimer[16, 17] and even trimer derivatives of PCBM.[9] Alternatively, groups have also used the technique of in-situ cross-linking with the introduction of small UV-curable bis-amide crosslinker[18] as well as PCBM based thermo-cross-linkers as an additive to the BHJ layer.[13, 19, 20] The inclusion or formation of these polymerized or multimer fullerenes have typically shown a significant improvement in the long-term stability of the OPV devices under simulated aging though the exact mechanism of lifetime improvement is not fully understood.[19]

In addition to controlling fullerene aggregation, understanding the diffusion of fullerene through the polymer in the bulk heterojunction devices is also important in the development of the device morphological structure, which ultimately plays a key role in determining the device efficiency.[7, 21-24] In order to understand how the donor (D)-acceptor (A) phase morphology in the bulk heterojunction layer affects device efficiencies a

a School of Materials Science and Engineering, Georgia Institute of Technology, Atlanta, GA 30332, USA
b School of Chemistry and Biochemistry, Georgia Institute of Technology, Atlanta, GA 30332, USA
c Center for Organic Photonics and Electronics (COPE), Georgia Institute of Technology, Atlanta, GA 30332, USA
d Department of Polymer Engineering, University of Akron, Akron, OH 44325
e. Current address: School of Engineering and Physical Sciences, Heriot-Watt University, Edinburgh, EH14 4AS, UK
Electronic Supplementary Information (ESI) available: includes details of synthesis, and analytical characterization, UV-vis absorption spectra, device characterization plots from P3HT and PBT7 systems, Avrami analysis, GIWAXS analysis, AFM plots s. See DOI: 10.1039/x0xx00000x

number of groups previously have studied model poly(alkylthiophene) (D) – fullerene (A) bulk heterojunction device structures and have observed three distinct layers in the bulk heterojunction.[25-29] Owing to fullerene diffusion through the polymer within the bulk-heterojunction, fullerene enriched layers are observed near the anode and cathode and consequently fullerene depletion (polymer enrichment) in the middle layer. It is thus important to systematically study the correlation of fullerene-polymer segregation in the active layer to the device performance.

Optimization of device performance is also often accompanied by annealing the device at temperatures typically well below the melting point of the polymer or fullerene for short periods of time. However, as discussed earlier, extended annealing or aging typically reduces the device performance.[8, 10] This owes to the fact that annealing directly affects the phase morphology of the polymer and fullerene blend in the BHJ. Previous studies on bilayer devices have shown that an initially pure layer of PCBM will diffuse through a pure P3HT layer within a few minutes when annealed at 150 ^{o}C.[21] Since the annealing temperature is well below T_m of the polymer or fullerene, but above the T_g of the polymer, diffusion of the fullerene occurs through the mobile amorphous phase of the polymer and grain boundaries.[21, 22] Due to its limited solubility in the amorphous polymer excess fullerene aggregates at elevated temperatures leading to significant degradation in device performance. Keeping these factors in mind, it is thus important to be able to study and eventually control the morphological development of the bulk heterojunction system.

Thus, the objective of this work is to develop a strategy to generate oligomeric fullerene derivatives in-situ in BHJs and study their diffusion behavior in comparison with monomeric PCBM.

Benzocyclobutene (BCB) is often used as a thermal cross-linking group, and undergoes oligomerization readily *via* a o-quinodimethane reactive intermediate in the presence of heat.[30-32] Previously, cycloaddition of o-quinodimethane onto fullerene in high boiling temperature solvents at reflux temperature gave fullerene based dimers, oligomers and polymers.[33, 34] These reactions however were carried out in solvents at high reflux temperatures and with long cross-linking reaction times. Using these reactions as a template, herein, we report a facile procedure for obtaining a fullerene with a cross-linkable benzocyclobutene moiety, which thermally cross-links in-situ to obtain fullerene oligomers. We chose our strategy of in-situ thermal cross-linking because unlike the final cross-linked fullerene, the monomeric fullerene precursor synthesized here is readily soluble, which allows us to use established processing conditions to fabricate the devices. We subsequently used the cross-linked fullerene to study the fullerene diffusion and aggregation behavior in bulk-heterojunction devices using P3HT as a donor in BHJs. The devices with the cross-linked fullerene show extremely good stability against thermal induced degradation, and device performance was correlated with the observed morphological behavior.

Results and discussion

Synthesis of thermal cross-linkable fullerene

Synthesis of PCBM related fullerene with a BCB thermal cross-linker was carried out as shown in Scheme 1. The starting materials of [6,6]-phenyl-C_{60}-butyric acid (PCBA), synthesized from commercially sourced PCBM (American Dye Source, inc.), and the 1-hydroxy benzocyclobutene (BCB-OH) were both synthesized following reported procedures.[2, 32, 35] The PCBA was subsequently reacted with BCB-OH under *N*,*N*′-

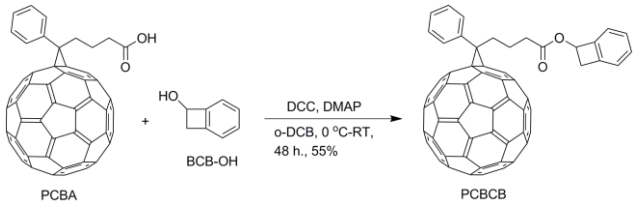

Scheme 1. Synthesis of PCBCB.

dicyclohexylcarbodiimide (DCC)-assisted esterification conditions in ortho-dichlorobenzene (o-DCB) in order to obtain the desired precursor product phenyl-C_{61}-butyric acid benzocyclobutene ester, (PCBCB) (see Scheme 1). PCBCB, which is readily soluble in common organic solvents, was purified though column chromatography and characterized by ^{1}H and ^{13}C NMR spectroscopy, mass spectrometry, high-performance liquid chromatography (HPLC) and elemental analysis. See Supporting Information for further details.

The fullerene cross-linked product ($(PCBCB)_n$) was formed in-situ from the purified PCBCB *via* thermal annealing. Mass spectral analysis of annealed PCBCB film showed the formation of fullerene dimer along with monomeric fullerene and other decomposition products (see supporting information). However, although formation of higher oligomeric and polymeric products may be possible, they were not observed in the mass spectral analysis, suggesting $(PCBCB)_n$, where n = 2 is the major product. Due to insolubility of the final cross-linked products, further structural characterization could not be carried out. However, results of thermally annealing different combinations of the precursor (PCBCB), PCBM and the BCB compounds and previous studies on these materials in literature [31, 32, 34, 36] lead us to suggest the possible reaction pathways for the formation of the final cross-linked fullerene products (i.e. $(PCBCB)_n$) (see supporting information).

Differential Scanning Calorimetry (DSC)

DSC analysis of the PCBCB in hermetically sealed Al pans was carried out from a start temperature of -50 ˚C up to 300 ˚C at a rate of 10 °C /min. The heating and cooling cycles are shown in Figure 1. The first cycle showed a strong exothermic peak, beginning at ~150 ˚C, indicative of an exothermic chemical reaction, associated with the crosslinking reaction of BCB.

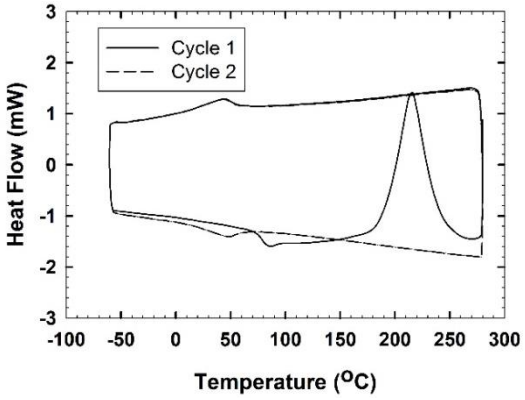

Figure 1. DSC thermogram of cross-linking reaction of PCBCB.

moieties. This is in good agreement with previously observed crosslinking temperatures also measured by DSC for other BCB-based thermally induced cross-linking reactions.[24]

UV-Vis spectra analysis

Absorption spectra of the PCBCB and PCBM in thin films were measured, before and after annealing at different temperatures (150, 190 and 230 °C) for 10 minutes. While PCBM showed no significant changes post annealing (Figure 2a), PCBCB showed a distinct reduction in the peak intensity at 360 nm, indicative of a change in the packing of the system beginning as low at 150 ˚C (Figure S8, possibly associated with onset of the cross-linking reaction as indicated by earlier DSC measurements). Subsequent annealing of the PCBCB at higher temperatures did not result in significant changes to the UV-visible absorption spectrum beyond those observed at 190 ˚C, (see Figure 2b), suggesting that all or the majority of the changes in the structure had already occurred at 190 ˚C and the cross-linking percentage was estimated to be close to 100% (see supporting information). Thus this was the temperature used subsequently for carrying out the cross-linking in thin films.

Fullerene-polymer diffusion behavior

An important part of controlling the morphology of BHJ systems is control of the diffusion of the fullerene through the polymer. Thus diffusion behavior of the $(PCBCB)_n$ fullerene into P3HT was compared to that of PCBM. Upon preparing bilayers of the fullerenes and P3HT (see experimental) the sulfur content through the BHJ film thickness was determined using XPS measurements as a function of the etching depths (which is proportional to the etching time) for various annealing times (Figure 3). The various depths were accessed by etching the film with an ion gun for fixed lengths of time. The samples were measured as unannealed bilayers and also after annealing for different amounts of time at 150 ˚C. In the pristine samples the two-layer structure is defined by a sharp but finite interface between the P3HT upper layer and the underlying fullerene. Diffusion of the fullerene through the polymer is characterized by loss of the initial interface to give a uniform distribution of the S through the film thickness (Figure 3). In a 1:1 ratio of the P3HT: fullerene the calculated S content in a homogeneous blend would be 4 (atomic) %, a value which both films prepared with PCBM and $(PCBCB)_n$ obtained after sufficient annealing times. PCBM has been known to diffuse quickly through the amorphous regions and the grain boundaries of P3HT upon various annealing conditions.[21, 22, 37] Thus in the PCBM system (Figure 3a), a homogeneous film composition was observed very quickly within 1 minute of annealing at 150 ˚C, which is consistent with previously reported studies.[21] By comparison, the $(PCBCB)_n$ (Figure 3b), shows negligible diffusion into P3HT for the first 15 minutes of annealing, although a homogeneous composition occurs at some time between 15 and 30 minutes annealing. This clearly shows that the diffusion rate of the $(PCBCB)_n$ that is at least an order of magnitude slower than PCBM.

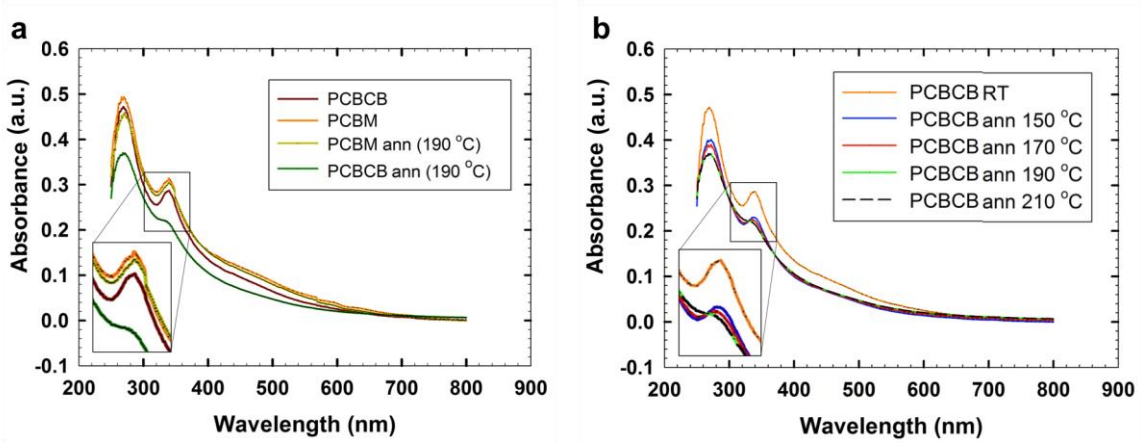

Figure 2. UV-Vis absorption spectra of, (a) unannealed and annealed thin films of PCBCB and PCBM, (b) PCBCB annealed at different temperatures (insets show the zoomed in areas inside the box; 'ann' in the captions indicates annealed films).

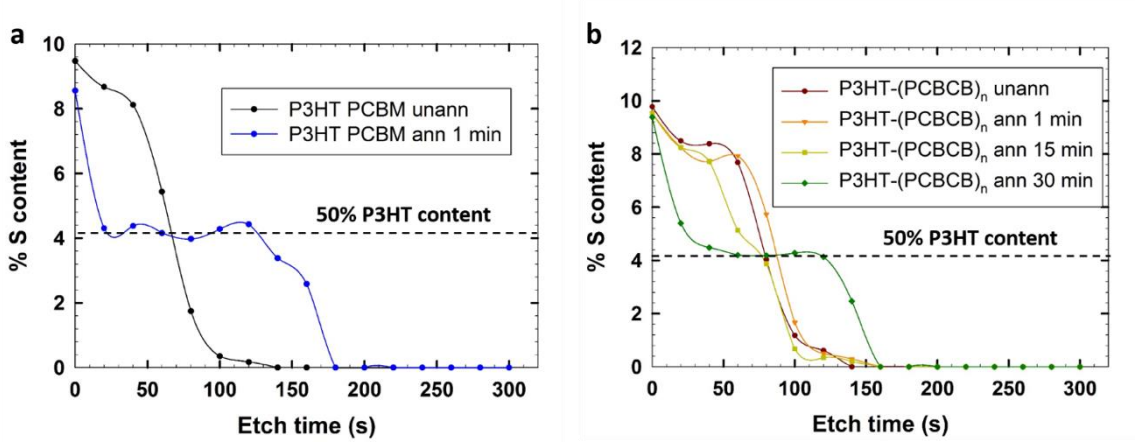

Figure 3. Percent Sulfur content through as a function of etch time, annealing at 150 °C for different amounts of time for (a) P3HT-PCBM bilayer and (b) P3HT-$(PCBCB)_n$ bilayer (unann – unannealed, ann-annealed).

Mobility, Electrochemical and Device Stability measurements

The electron mobility values of the fullerenes were determined from space charge limited current (SCLC) measurements (see Figure S9, results in Table 1). These measurements showed that compared to PCBM the PCBCB precursor has a slightly lower, but comparable electron mobility values. The electron mobility value for PCBCB though does increase significantly upon the crosslinking reaction to give $(PCBCB)_n$. To get a better understanding and possible explanation of this enhancement of electron mobility, GIWAXS measurements were carried out to compare the crystal structures and are summarized in the supporting information (see section on GIWAXS).

To estimate the LUMO energy level of PCBCB, cyclic-voltammetry experiments were carried out and showed negligible change in its reduction potential values with respect to PCBM (see supporting information), indicating its LUMO energy level is similar to the PCBM. Due to its insolubility, we were not able to carry out electrochemical measurements on $(PCBCB)_n$. Given the similar electron mobility values for the PCBM and $(PCBCB)_n$, BHJ devices were made with these materials as acceptors and P3HT as the donor molecule. A third device was also made with a 1:1 ratio of PCBM: $(PCBCB)_n$ as the acceptor. The devices were annealed for 10 minutes each at 190 °C to allow for the cross-linking of PCBCB to occur following the spin coating of the active layer and before the aluminum electrode was deposited. The PCBM and $(PCBCB)_n$ based devices showed comparable efficiencies as made, with the cross-linked fullerene showing only a slightly reduced initial efficiency. These devices were subsequently aged at 150 °C for increasing periods of time (up to 48 hours or 2880 minutes) and the efficiencies of all three devices measured at regular intervals (Figure 4). It was observed that the P3HT-PCBM based samples begin to degrade substantially within 1 hour of aging, and very quickly thereafter show only 40% of their initial efficiency, as seen previously in a number of other studies.[38-40]

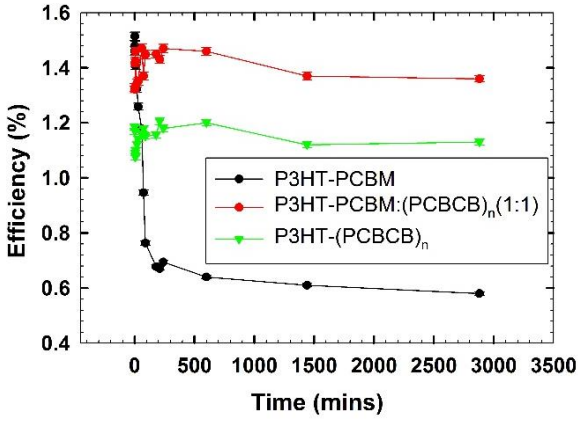

Figure 4. Device efficiency as function of aging time for P3HT-fullerene BHJs where the fullerenes are PCBM (black), 1:1 PCBM: $(PCBCB)_n$ blend (red) and $(PCBCB)_n$ (green).

By comparison, the devices where the acceptor was a 1:1 ratio PCBM: $(PCBCB)_n$ blend or pure $(PCBCB)_n$ initially showed a slight increase and then a stable value of the device efficiency. More importantly neither of the devices containing $(PCBCB)_n$ showed any effective degradation in the device efficiency (compared to its initial device efficiency) even when aged for up to 48 hours at elevated temperatures. The devices themselves were not as efficient as reported by other sources previously due to the selection of a non-optimized polymer: fullerene ratio and absence of Calcium interlayer. However, this did provide us with a simpler device structure to study with the other characterization techniques.

Table 1. Electron mobility values (SCLC) for the different fullerenes (thickness – 210 nm)

Material	μ (cm^2/Vs)
PCBM	$9.1\pm1.0 \times 10^{-4}$
PCBCB	$1.3\pm0.3 \times 10^{-4}$
$(PCBCB)_n$	$5.9\pm1.8 \times 10^{-3}$

Fullerene crystal and aggregation growth

Nano-scale aggregates in the as-made BHJ samples are observed using AFM images (Fig S.13), suggesting that devices have an appropriate aggregate size to facilitate good device mobility and performance.[7] Upon aging however, the PCBM aggregates become too large in size to be viewed using the AFM imaging. Thus to study the effect of aging on fullerene crystallization, GIWAXS measurements were also carried out on the thin films of PCBM and $(PCBCB)_n$ aged for different amounts of time. The 2-D GIWAXS images of the fullerenes showed differences before and after annealing it for 1 h (Figure 5). In the case of PCBM, upon annealing, distinct crystalline peaks of the fullerenes from possible re-crystallization and subsequent large-scale aggregation, had replaced the initial amorphous halos. In contrast, the GIWAXS image for the annealed $(PCBCB)_n$ films did not show a significant change in the crystalline behavior suggesting a tendency not to re-crystallize even after prolonged annealing at elevated temperatures (aging at 150 ˚C Fig S12 b and Table S4). The crystallization kinetics were subsequently observed and measured using optical microscopy and the BHJs with fullerenes in different ratios (pure PCBM, PCBM: $(PCBCB)_n$ in 1:1 ratio and pure $(PCBCB)_n$) were compared. During aging of the P3HT-PCBM sample, formation of a large number of macroscopic-sized crystallites is observed (Figure 6).

These crystals are believed to be aggregates of fullerene as described before in the literature and indicated by the GIWAXS results of the prolonged aged PCBM thin films (Figure 5b).[8, 9, 24] This aggregation behavior forming macroscopic fullerene crystals has been shown to lead to the decrease of the different polymer-fullerene based BHJ device efficiency when the device is kept at high temperature over time, and explains the loss in device efficiency in this system.[6, 8, 41] When the PCBM is partly or completely replaced by $(PCBCB)_n$ as the acceptor the number density of fullerene crystallites formed

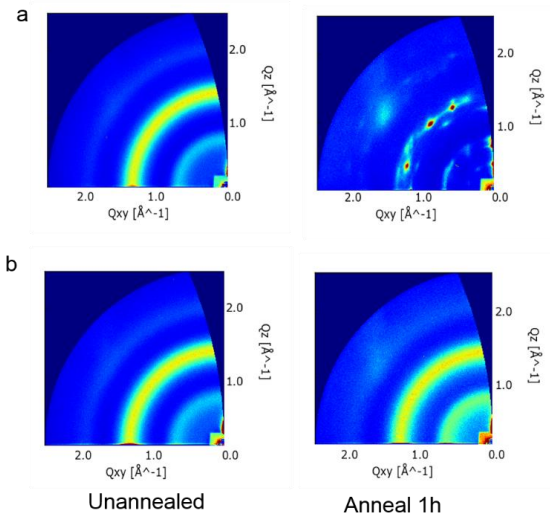

Figure 5. GIWAXS patterns for thin films of a) PCBM and b) $(PCBCB)_n$ before (left column) and after (right column) one hour of aging at 150 ºC.

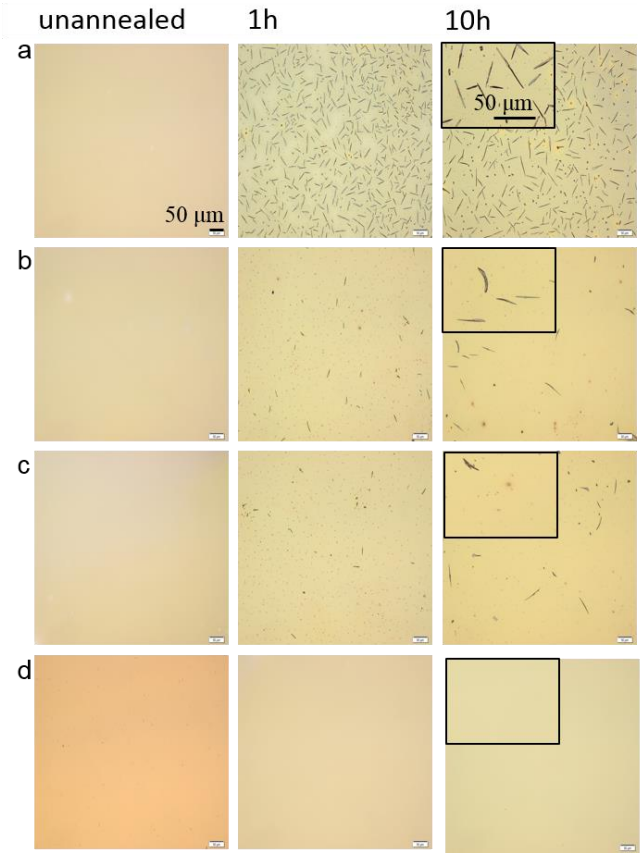

Figure 6. Optical microscopy images of P3HT-Fullerene thin films, before and after aging at 150 °C for 1 h, 10 h a) P3HT-PCBM b)P3HT-$(PCBCB)_n$:PCBM (1:3) c) P3HT-$(PCBCB)_n$:PCBM (1:1) d) P3HT-$(PCBCB)_n$ (insets of the images at 10 hrs show 3x zoom of a part of the image).

(measured as the percentage area of fullerene crystallites) was observed to decrease with increasing amount of $(PCBCB)_n$ in the system (Figure 7). This suggests that the $(PCBCB)_n$ actively inhibits the aggregation and crystallization of the PCBM molecules. This is assisted by the order of magnitude lower diffusion rate of $(PCBCB)_n$ in the P3HT compared to the PCBM. This diffusion rate inhibits rapid mobility and hence reduces aggregation of the fullerenes in the system leading to higher lifetimes of the devices even under elevated temperatures.

By analyzing the crystallite size as a function of aging time (Figure S11) and fitting using the Avrami equation (Equation S2) the fullerene crystallization growth rate in the active layers were obtained. Since pure $(PCBCB)_n$ based devices barely showed any visible aggregation or re-crystallization (as also observed in the GIWAXS measurements) Avrami analysis was not possible in this case. However, the calculated Avrami exponents in the systems containing pure PCBM and PCBM: $(PCBCB)_n$ (1:1) showed values close to 2 suggesting a 2-dimensional growth (Table 2). At the same time the rate constant calculated for the crystal growth however was, as anticipated, significantly lower when PCBM:$(PCBCB)_n$ (1:1) was used as an acceptor, as compared to just pure PCBM,

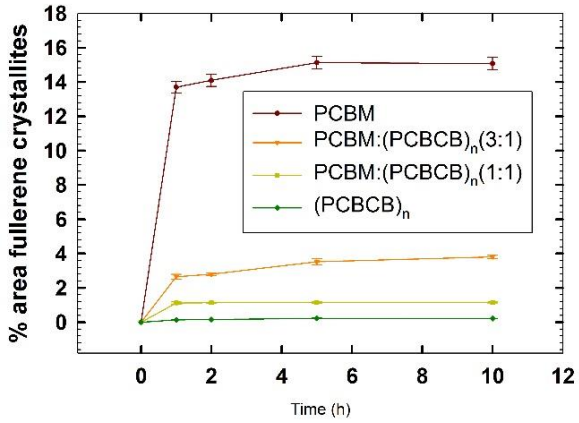

Figure 7. Percentage area of fullerene crystallites in BHJs with time, aged at 150˚C.

consistent with our hypothesis that introduction of a cross-linked fullerene is inhibiting the rate of growth of the PCBM crystals. Thus the reduction in crystal growth and aggregation arises from the introduction of the $(PCBCB)_n$ as a slow diffusing aggregation inhibiting agent.

An obvious question to ask is how universal is this approach. To partly answer this, we have made preliminary measurements of OPV device performance with BHJs containing the higher efficiency polymer, PTB7. Results show (Figure S14, Table S5) that devices with either $PC_{60}BM$ or $(PCBCB)_n$ fullerenes have very similar performance to each other and are entirely consistent with results previously reported in the literature.[42] As yet long term stability of these and other devices containing $(PCBCB)_n$ have yet to be undertaken, but will constitute part of future studies to expand the applicability of these cross-linking acceptor systems.

Table 2. Avrami exponent and Rate constants from Avrami Fits

Sample	Avrami Exponent	Rate Constant
P3HT-PCBM	1.89	0.31
P3HT-(PCBM:$(PCBCB)_n$) (3:1)	2.01	0.19
P3HT-(PCBM:$(PCBCB)_n$) (1:1)	2.11	0.16

Conclusions

We have synthesized a new thermal cross-linkable PCBM based molecule, which was thermally cross-linked in-situ to obtain an oligomeric fullerene derivative that has electron mobility comparable to the original PCBM. The use of these cross-linked fullerenes in bulk heterojunction based OPVs show comparable device efficiencies as well as a significant improvement in the device lifetime on being subjected to accelerated aging conditions. This behavior has been attributed to the reduction in the diffusion, and aggregation of this new fullerene in the devices. Similar fullerene based oligomeric acceptors are also being synthesized in the future with other BCB based cross-linker groups to allow crosslinking at even lower temperatures.

Acknowledgements

Work was partially supported by the Department of the Navy, Office of Naval Research Award Numbers N00014-14-1-0126 and N00014-14-1-0580. We also gratefully acknowledge partial support from by the U.S. Department of Energy, Division of Basic Energy Sciences under contract No. DE-FG02-10ER4779. We would also like to thank Dr. Chris Tassone for his help with the GIWAXS experiments at the SSRL, Stanford, USA.

Experimental Methods

Thin films were prepared for all characterization measurements (optical microscopy, UV-Vis measurement, BHJ devices for efficiency measurements and SCLC devices for electron mobility measurements, XPS for diffusion measurements), by spin coating solutions from o-dichlorobenzene (o-DCB) onto glass slides. Before use all glass slides were washed with surfactant solution, acetone and isopropanol, consecutively, and after drying the glass surfaces with N_2 gas, were UV-ozone cleaned.

UV-vis absorption measurements were carried out using a Varian Cary 5E UV-vis-NIR spectrophotometer with wavelength ranging from 300-800 nm. Optical microscopy measurements were carried out on an Olympus BX15 optical microscope with 20x zoom. Images were analyzed using ImageJ v1.48.

Thin films for GIWAXS, optical microscopy and UV-vis measurement were prepared from different solutions made from pure PCBM and PCBCB, and also BHJ blends with P3HT. The P3HT: fullerene ratio in the BHJ layers was kept as 1:1 in all of the films. Films were spun from 20 mg/ml solutions in o-dichlorobenzene solutions (500 RPM for 2 sec followed by 800 RPM for 50 seconds) onto microscope glass slides.

Thin films for OPV device measurements were made on ITO covered glass slides. A layer of PEDOT: PSS was first deposited onto the ITO by spin coating a PEDOT: PSS solution (Clevios Al4083 by Heraeus) at 4000 RPM for 45 seconds. Films were subsequently annealed for 10 minutes at 150 ˚C in a glove box. The active layer was made of P3HT/fullerene blends in a weight ratio of 1:1, with the fullerene being pure PCBM, PCBCB or PCBM: PCBCB in a 1:1 ratio. The active layer was spin coated from 20 mg/ml o-DCB solutions (500 RPM for 2 seconds followed by 800 RPM for 50 seconds). All active layer films were annealed at 190 ˚C for 10 minutes. Finally, a 100 nm Al electrode layer was deposited on to the BHJ using thermal evaporation technique under vacuum. Subsequently, the devices were aged on a hot plate in the glove box at 150 ˚C for varying amounts of time and the OPV efficiency determined at room temperature using a Keithley's Series 2400 SMU source meter under an AM 1.5 solar spectrum.

SCLC measurements were performed on devices that were built on pre-patterned ITO. The pre-patterned slides were ultrasonicated in sodium dodecyl sulfate and water for 10 minutes, followed by a water rinse. Afterwards, ITO was

ultrasonicated in acetone, then isopropanol for 10 minutes each. ITO was then UV-ozone cleaned for 10 minutes. PEDOT: PSS (Al 4083) was filtered through a 0.45 µm nylon filter and spincoated onto the cleaned ITO at 5000 rpm for 60 seconds. PEDOT: PSS coated devices were then transferred into an Ar filled glovebox and annealed at 120 °C for 15 minutes. Solutions of fullerene with concentrations of 30 mg/mL in chloroform were spin coated onto PEDOT: PSS devices at 1200 rpm for 60 seconds. Subsequently the devices were placed in a thermal evaporator where 1 nm of LiF was deposited, followed by 80 nm of Al. Devices were tested using a Keithley's Series 2400 SMU source meter. Film thicknesses were measured using a Bruker stylus profilometer.

Bilayers for the XPS diffusion measurements were made by first spin coating a layer of fullerene (20 mg/ml in o-DCB), onto a glass slide (500 RPM for 2 seconds followed by 800 RPM for 50 seconds). In case of the PCBCB film, this was then annealed at 190 ˚C for 10 minutes to allow the cross-linking reaction. The P3HT layers were prepared by spinning onto different glass slides that were initially spin coated with PEDOT: PSS. The P3HT polymers were then floated off onto water (to dissolve the PEDOT: PSS and release the P3HT film), which were then transferred onto the fullerene layer. The resulting bilayer structure was subsequently air dried until no visible water traces remained and then vacuum dried at RT overnight. XPS measurements were performed in the shared user laboratory of the Georgia Tech IEN Organic Cleanroom. The machine used was a Thermo K-alpha XPS. The etching was carried out using a Argon ion source at an energy of 3000 eV, with constant etch time of 20 sec in each etch cycle, i.e. between subsequent measurements. GIWAXS measurements were carried out on beamline 11-3 at the Stanford synchrotron radiation light source (SSRL). The beam was kept at an energy of 13 KeV and the critical angle of measurement was 0.12°. A LaB_6 standard sample was used to calibrate the instrument and the software WxDiff was used to reduce the 2-D scattering data into the corrected 1-D integration plots (I vs q).

Notes and references

1. N. S. Sariciftci, L. Smilowitz, A. J. Heeger and F. Wudl, *Science*, 1992, **258**, 1474-1476.
2. J. C. Hummelen, B. W. Knight, F. LePeq, F. Wudl, J. Yao and C. L. Wilkins, *The Journal of Organic Chemistry*, 1995, **60**, 532-538.
3. H. Hoppe and N. S. Sariciftci, *Journal of Materials Chemistry*, 2006, **16**, 45-61.
4. C. J. Brabec, S. Gowrisanker, J. J. M. Halls, D. Laird, S. Jia and S. P. Williams, *Advanced Materials*, 2010, **22**, 3839-3856.
5. F. Liu, Y. Gu, J. W. Jung, W. H. Jo and T. P. Russell, *Journal of Polymer Science Part B: Polymer Physics*, 2012, **50**, 1018-1044.
6. X. Yang, J. K. J. van Duren, R. A. J. Janssen, M. A. J. Michels and J. Loos, *Macromolecules*, 2004, **37**, 2151-2158.
7. W.-R. Wu, U. S. Jeng, C.-J. Su, K.-H. Wei, M.-S. Su, M.-Y. Chiu, C.-Y. Chen, W.-B. Su, C.-H. Su and A.-C. Su, *ACS Nano*, 2011, **5**, 6233-6243.
8. S. Miyanishi, K. Tajima and K. Hashimoto, *Macromolecules*, 2009, **42**, 1610-1618.
9. K. Sivula, C. K. Luscombe, B. C. Thompson and J. M. J. Fréchet, *Journal of the American Chemical Society*, 2006, **128**, 13988-13989.
10. J. J. Richards, A. H. Rice, R. D. Nelson, F. S. Kim, S. A. Jenekhe, C. K. Luscombe and D. C. Pozzo, *Advanced Functional Materials*, 2013, **23**, 514-522.
11. C. Lindqvist, J. Bergqvist, O. Bäcke, S. Gustafsson, E. Wang, E. Olsson, O. Inganäs, M. R. Andersson and C. Müller, *Applied Physics Letters*, 2014, **104**, 153301.
12. M.-H. Liao, C.-E. Tsai, Y.-Y. Lai, F.-Y. Cao, J.-S. Wu, C.-L. Wang, C.-S. Hsu, I. Liau and Y.-J. Cheng, *Advanced Functional Materials*, 2014, **24**, 1418-1429.
13. Y.-J. Cheng, C.-H. Hsieh, P.-J. Li and C.-S. Hsu, *Advanced Functional Materials*, 2011, **21**, 1723-1732.
14. Z. Li, H. C. Wong, Z. Huang, H. Zhong, C. H. Tan, W. C. Tsoi, J. S. Kim, J. R. Durrant and J. T. Cabral, *Nat Commun*, 2013, **4**.
15. H. C. Wong, Z. Li, C. H. Tan, H. Zhong, Z. Huang, H. Bronstein, I. McCulloch, J. T. Cabral and J. R. Durrant, *ACS Nano*, 2014, **8**, 1297-1308.
16. B. C. Schroeder, Z. Li, M. A. Brady, G. C. Faria, R. S. Ashraf, C. J. Takacs, J. S. Cowart, D. T. Duong, K. H. Chiu, C.-H. Tan, J. T. Cabral, A. Salleo, M. L. Chabinyc, J. R. Durrant and I. McCulloch, *Angewandte Chemie International Edition*, 2014, **53**, 12870-12875.
17. J. Liu, X. Guo, Y. Qin, S. Liang, Z.-X. Guo and Y. Li, *Journal of Materials Chemistry*, 2012, **22**, 1758-1761.
18. J. W. Rumer, R. S. Ashraf, N. D. Eisenmenger, Z. Huang, I. Meager, C. B. Nielsen, B. C. Schroeder, M. L. Chabinyc and I. McCulloch, *Advanced Energy Materials*, 2015, **5**, n/a-n/a.
19. G. Wantz, L. Derue, O. Dautel, A. Rivaton, P. Hudhomme and C. Dagron-Lartigau, *Polymer International*, 2014, **63**, 1346-1361.
20. M. Drees, H. Hoppe, C. Winder, H. Neugebauer, N. S. Sariciftci, W. Schwinger, F. Schaffler, C. Topf, M. C. Scharber, Z. Zhu and R. Gaudiana, *Journal of Materials Chemistry*, 2005, **15**, 5158-5163.
21. D. Chen, F. Liu, C. Wang, A. Nakahara and T. P. Russell, *Nano Letters*, 2011, **11**, 2071-2078.
22. N. D. Treat, M. A. Brady, G. Smith, M. F. Toney, E. J. Kramer, C. J. Hawker and M. L. Chabinyc, *Advanced Energy Materials*, 2011, **1**, 82-89.
23. B. Watts, W. J. Belcher, L. Thomsen, H. Ade and P. C. Dastoor, *Macromolecules*, 2009, **42**, 8392-8397.
24. M. Campoy-Quiles, T. Ferenczi, T. Agostinelli, P. G. Etchegoin, Y. Kim, T. D. Anthopoulos, P. N. Stavrinou, D. D. C. Bradley and J. Nelson, *Nat Mater*, 2008, **7**, 158-164.
25. D. S. Germack, C. K. Chan, B. H. Hamadani, L. J. Richter, D. A. Fischer, D. J. Gundlach and D. M. DeLongchamp, *Applied Physics Letters*, 2009, **94**, 233303.
26. D. Chen, A. Nakahara, D. Wei, D. Nordlund and T. P. Russell, *Nano Letters*, 2010, **11**, 561-567.
27. S. S. van Bavel, M. Bärenklau, G. de With, H. Hoppe and J. Loos, *Advanced Functional Materials*, 2010, **20**, 1458-1463.
28. A. J. Parnell, A. D. F. Dunbar, A. J. Pearson, P. A. Staniec, A. J. C. Dennison, H. Hamamatsu, M. W. A. Skoda, D. G. Lidzey and R. A. L. Jones, *Advanced Materials*, 2010, **22**, 2444-2447.

29. J. W. Kiel, B. J. Kirby, C. F. Majkrzak, B. B. Maranville and M. E. Mackay, *Soft Matter*, 2010, **6**, 641-646.
30. B. Ma, F. Lauterwasser, L. Deng, C. S. Zonte, B. J. Kim, J. M. J. Fréchet, C. Borek and M. E. Thompson, *Chemistry of Materials*, 2007, **19**, 4827-4832.
31. J. N. Dobish, S. K. Hamilton and E. Harth, *Polymer Chemistry*, 2012, **3**, 857-860.
32. J. L. Segura and N. Martín, *Chemical Reviews*, 1999, **99**, 3199-3246.
33. A. Kraus, A. Gügel, P. Belik, M. Walter and K. Müllen, *Tetrahedron*, 1995, **51**, 9927-9940.
34. A. Gügel, P. Belik, M. Walter, A. Kraus, E. Harth, M. Wagner, J. Spickermann and K. Müllen, *Tetrahedron*, 1996, **52**, 5007-5014.
35. W. Bubb and S. Sternhell, *Australian Journal of Chemistry*, 1976, **29**, 1685-1697.
36. C. Pugh, J. S. Baker and W. K. Storms, *Synlett*, 2014, **25**, 148-152.
37. N. D. Treat, T. E. Mates, C. J. Hawker, E. J. Kramer and M. L. Chabinyc, *Macromolecules*, 2013, **46**, 1002-1007.
38. M. Jørgensen, K. Norrman and F. C. Krebs, *Solar Energy Materials and Solar Cells*, 2008, **92**, 686-714.
39. Y. Zhang, H.-L. Yip, O. Acton, S. K. Hau, F. Huang and A. K. Y. Jen, *Chemistry of Materials*, 2009, **21**, 2598-2600.
40. J. U. Lee, J. W. Jung, T. Emrick, T. P. Russell and W. H. Jo, *Journal of Materials Chemistry*, 2010, **20**, 3287-3294.
41. N. Camaioni, M. Catellani, S. Luzzati and A. Migliori, *Thin Solid Films*, 2002, **403–404**, 489-494.
42. A. Guerrero, N. F. Montcada, J. Ajuria, I. Etxebarria, R. Pacios, G. Garcia-Belmonte and E. Palomares, *Journal of Materials Chemistry A*, 2013, **1**, 12345-12354.